Available online at www.sciencedirect.com
SCIENCE DIRECT
Cement and Concrete Research 36 (2006) 625 – 633
Cement and Concrete Research

Correlation between porosity, permeability and ultrasonic parameters of mortar with variable water/cement ratio and water content

Zoubeir Lafhaj [a,*], Marc Goueygou [b], Assia Djerbi [a], Mariusz Kaczmarek [c]

[a] LML UMR CNRS 8107, Ecole Centrale de Lille, Villeneuve d'Ascq, France
[b] IEMN DOAE UMR CNRS 8520, Ecole Centrale de Lille, Villeneuve d'Ascq, France
[c] Institute of Environmental Mechanics and Applied Computer Science, Bydgoszcz, University, Poland

Received 9 February 2005; accepted 9 November 2005

Abstract

This paper presents results of studies of ultrasonic and structural parameters of mortar. The objective of the study is to determine correlations between ultrasonic pulse velocity (UPV), porosity and permeability. The material investigated consists in seven mortar mixtures with water/cement ratio varying from 0.3 to 0.6. The paper is composed of three parts. The first one presents a description of the mortar samples that were subjected to ultrasonic, porosity and gas permeability tests and describes the details of those tests. Then, a simple model is proposed to relate ultrasonic pulse velocity with porosity and permeability. Finally, experimental results are shown and correlations between the measured parameters of the material are discussed. In the range of porosity values considered, the model correctly describes the dependence of UPV versus porosity and permeability. It could thus be used to predict the evolution of structural parameters of the material from non-destructive measurements.

Keywords: Mortar; Non-destructive testing; Permeability; Porosity; Ultrasound

1. Introduction

Deterioration of concrete structures is generally caused by penetration of aggressive agents (sulphates, chlorides, moisture, CO_2,...) into the concrete interior. Thus, concrete durability is strongly related to the quality of its cover, which corresponds to the first few centimeters of material below the surface of the structure. Porosity and permeability are widely recognized durability indices, since they quantify the resistance of the material against penetrating agents [3]. Current on site absorption and permeability tests are based on measurements of liquid or airflow. They include capillary suction, initial surface absorption test (ISAT) and Figg test [4]. On the other hand, ultrasonic methods have been used since the mid 1940's for concrete testing. The most commonly measured parameter is the ultrasonic pulse velocity (UPV). Ultrasonic attenuation (UA) is less frequently used for concrete characterization, as the material heterogeneity makes it difficult to measure [12,13,29]. So far, ultrasonic methods have been used for estimating concrete strength through UPV measurement [24–26], and to detect internal defects (voids, cracks, delaminations,...) [17]. Recently, an ultrasonic test has been developed for non-destructive durability assessment to chloride ion penetration [28,30]. It is based on correlations established between UPV, porosity and permeability, which were shown to be coherent with theoretical models [32]. The successful application of this test means that ultrasonic methods can be effectively used to investigate a wide range of properties in concrete, including its durability indices.

Following a similar procedure, this study intends to establish correlations between ultrasonic parameters and selected durability indices (porosity and permeability) of dry, partially and fully saturated mortar samples. Compared to the work of Aktan and co-workers, a few features are added. First, the frequency range is significantly higher: 0.5 MHz for the initially emitted ultrasonic pulse, compared to the 50 kHz frequency generally used for concrete testing. One reason is to increase the sensitivity of propagation parameters, especially attenuation, to the changes of microstructure [20]. Another

* Corresponding author.
E-mail address: zoubeir.lafhaj@ec-lille.fr (Z. Lafhaj).

0008-8846/$ - see front matter © 2005 Elsevier Ltd. All rights reserved.
doi:10.1016/j.cemconres.2005.11.009

Table 1
Proportion of the mortar constituents

Constituent	Proportion (kg/m^3)
Cement	639
Fine sand (0.16–2 mm)	966
Coarse sand (0.8–3.15 mm)	414

reason is related to the development of a surface wave technique for concrete cover inspection [11]. Ultrasonic parameters are the UPV of both longitudinal and shear waves, so dynamic elastic moduli can be estimated. Ultrasonic attenuation of both waves are also measured here, and their variation with porosity and permeability is shown. Finally, in contrast with the Rapid Chloride Permeability Test (RCPT) used by Udegbunam et al. [30], a direct measurement of gas permeability was performed.

We start with a description of the mortar samples that were subjected to ultrasonic, porosity and gas permeability tests. The next section presents the details of those three tests. Then, theoretical relationships between UPV, porosity and permeability are formulated. Next, experimental results are discussed and correlations between the measured parameters of the material are established.

2. Materials

In order to obtain various porosity and permeability values, mortar samples were fabricated with different water/cement (w/c) ratios. In addition, the samples were either dry, fully or partially saturated with water. Mortar was chosen instead of concrete, first, to limit excessive attenuation of ultrasonic waves due to scattering by large grains, and second, because mostly smaller grains are present in the first millimeters of the concrete cover. The samples are cylinders of diameter 37 and 10 mm height. The thickness was chosen to be small enough so as to allow transmission of the ultrasonic wave with initial central frequency of 0.5 MHz. They were cored from larger cylinders preserved over 28 days in a water solution of lime at a constant temperature of 20 °C, and then rectified to make the sample faces smooth and parallel. The mortar used is of a fine grain type, made up of Portland cement CPA CEM I 52.5 from Origny and Hostun sand. The mixture is prepared with seven different w/c ratios, ranging from 0.3 to 0.6. Table 1 gives the proportions of the various constituents.

The conditioning consists in storing the samples in an air-conditioned room at 60 °C temperature. The time of storage is the main parameter which influences the hydrothermal conditions of the sample. The water content of the sample was determined by measuring the difference between the weight at saturated conditions and the weight at a given drying time. The delay between the time when the sample is taken out from the air-conditioned room and the time of the test is short enough to have no significant influence on its water content. Three ranges of saturation were considered: Full saturation (FS) when the water content is more than 85% of the fully saturated specimen, partial saturation (PS) when it is in between 45% and 55% and dry (D) when the saturation is less than 10%. Fig. 1 presents the variation of the saturation of the sample with the drying time. For example, according to that figure, measurements should be carried out after two days of drying if we would like to evaluate specimens with 50% saturation.

3. Experimental setup

3.1. Ultrasonic test

Broadband ultrasound spectroscopy [10] was used to obtain ultrasonic parameters of the materials. Here, this technique is applied in pulse-echo mode, using a single transducer working as both transmitter and receiver. The initially emitted ultrasonic pulse is wideband, with a central frequency of 1 MHz and a 70% bandwidth. However, due to the low-pass filtering effect induced by increasing frequency material attenuation, the spectrum of the received signal has significant energy between 0.5 and 1 MHz, with a maximum around 0.65 MHz. To generate the electrical pulse and amplify the received signal, a Panametrics 5055 pulser–receiver is used. The amplified signal is then digitized at 250 MHz by a digital oscilloscope and stored on a PC. Adequate coupling is required to transfer enough energy into the sample. Instead of immersion coupling, direct contact was chosen to avoid uncontrolled water penetration into the sample during the ultrasonic test. In this study, pulse velocity and attenuation are measured using the buffer rod method [22,23]. This method allows unbiased

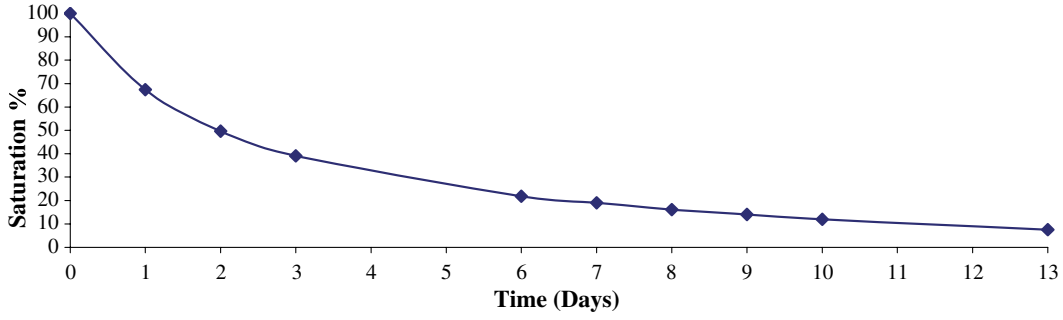

Fig. 1. Drying curve of mortar sample with 0.4 w/c ratio.

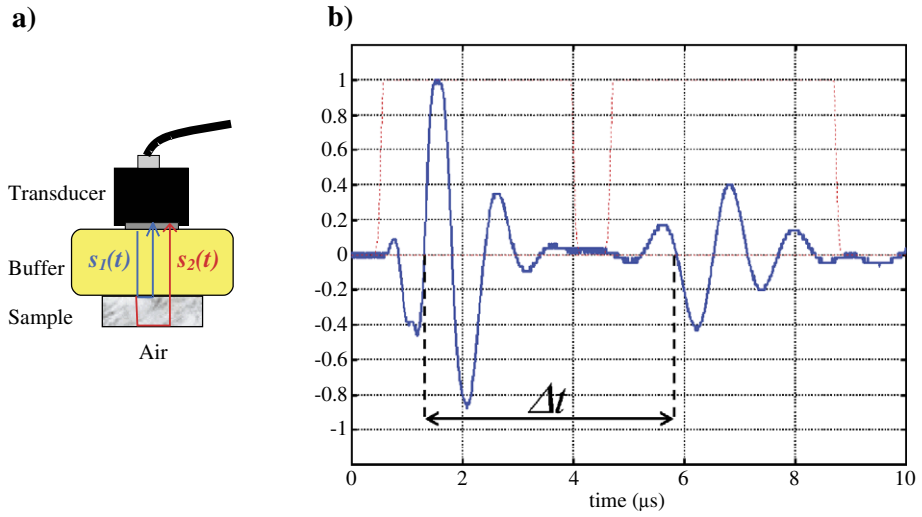

Fig. 2. Measurement of pulse velocity. a) Measurement setup; b) Reflected pulses (solid line), time windows (dotted line) and estimation of time delay Δt.

attenuation estimates by eliminating the influence of transducer coupling that occurs in direct contact transmission mode. It consists in introducing a 10 mm thick Plexiglas buffer between the transducer and the sample. A thin layer of coupling agent is applied at the transducer/buffer and at the buffer/sample interfaces. It is either a silicone gel (Sofranel D couplant) for longitudinal waves or a highly viscous liquid (Sofranel SWC couplant) for transverse waves.

First, pulse velocity is obtained as:

$$V_{L,T} = \frac{2e}{\Delta t} \tag{1}$$

where e is the thickness of the sample and Δt is the time delay between signals $s_1(t)$ and $s_2(t)$ (Fig. 2a). Signal $s_1(t)$ corresponds to the reflection of the incident wave at the interface between the bottom of the buffer and the top of the sample; signal $s_2(t)$ is the echo from the bottom of the sample. Since the pulse duration (3.3 μs which corresponds to 2 periods at 0.6 MHz) is smaller than time delay Δt (4 μs at least for the highest velocity), signals $s_1(t)$ and $s_2(t)$ can be easily separated by time windowing (Fig. 2b). Moreover, as reflection at the sample bottom causes a phase shift of the backwall echo relative to the emitted signal, the time references for estimating Δt were the positive-slope and negative-slope zero-crossings for signal $s_1(t)$ and $s_2(t)$ respectively (Fig. 2b). Measurement of attenuation consists in two steps. First, the backwall echo from the buffer is recorded without sample (Fig. 3a), yielding a reference signal with amplitude spectrum denoted as $S_0(f)$. Second, the sample was coupled to the buffer (Fig. 3b) and signals $s_1(t)$ and $s_2(t)$ were recorded. After time windowing (Fig. 2b), their amplitude spectra $S_1(f)$ and $S_2(f)$ are obtained. Finally, attenuation was derived from the following equation:

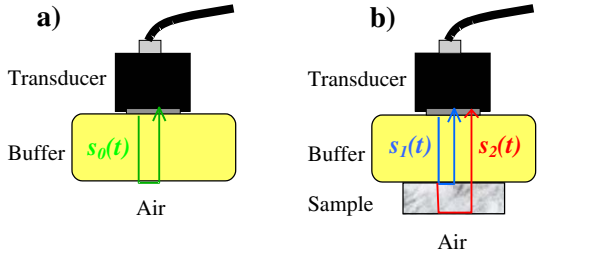

Fig. 3. Measurement of attenuation. a) Buffer response; b) Buffer-sample response.

$$\alpha(f) = \frac{1}{2e}\left\{\ln\left[\frac{S_0(f)\left(1-R(f)^2\right)}{S_2(f)}\right]\right\} \tag{2}$$

with $R(f) = \frac{S_1(f)}{S_0(f)}$ as the buffer/sample reflection coefficient. As we are mainly interested in relative variation of attenuation with w/c ratio and water content rather than in absolute attenuation values, no diffraction correction was made on attenuation curves. Finally, a unique value was extracted for each material by estimating the attenuation slope (in dB/cm/MHz) using a linear regression of the attenuation curve $\alpha(f)$ within the signal bandwidth (Fig. 4).

3.2. Porosity and gas permeability tests

Porosity was measured by the gravity method, using vacuum saturation. This method consists in submitting the sample to moderate oven-drying at a temperature of 60 °C [15]. The drying is stopped when the weight of the sample remains constant. Porosity (p) was determined using the following formula:

$$p = \frac{M_{sat} - M_{dry}}{\rho_w V_{vol}} \tag{3}$$

where ρ_w is the volume density of water, V_{vol} is the volume of the sample, M_{dry} and M_{sat} denote respectively the weight of the dried and fully saturated sample.

The general principle of the permeability test is to apply a continuous gas flow through the sample under steady conditions

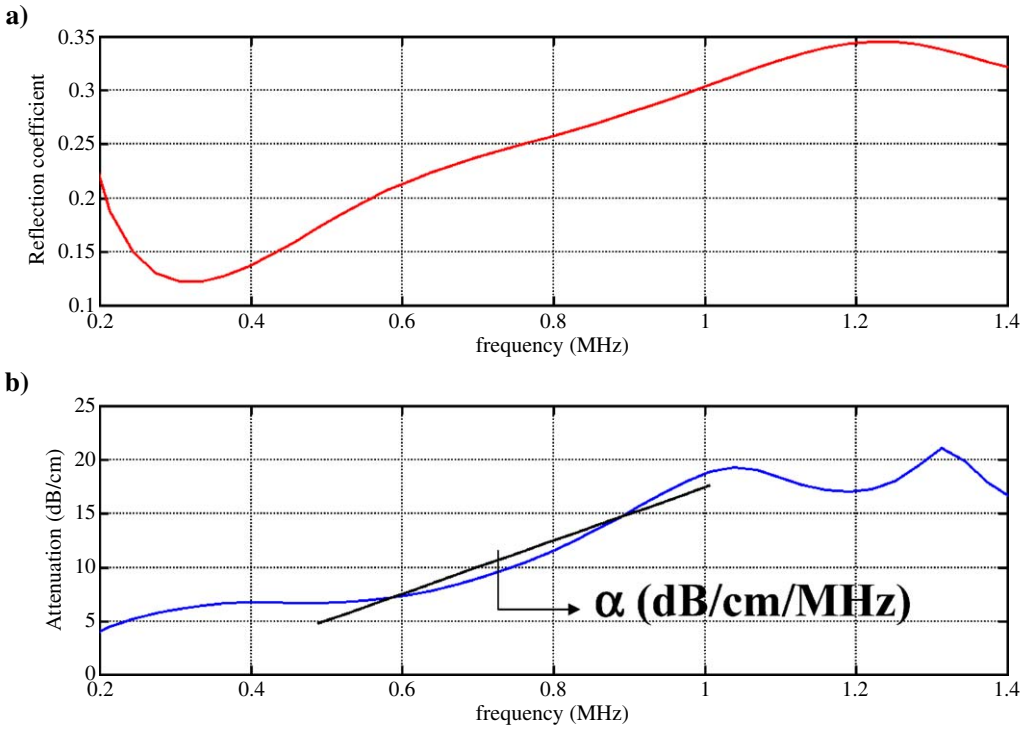

Fig. 4. Result of attenuation measurement. a) Reflection coefficient $R(f)$; b) Attenuation curve $\alpha(f)$ and its slope in the 0.5–1 MHz frequency range.

[7]. The gas injected is argon, which is assumed to be an ideal gas [14]. The pressure cell was designed to submit the sample to a constant gas pressure P_i at one end and to atmospheric pressure P_0 at the other end. Fig. 5 shows an overall diagram of the experimental setup. The latter enables permeability values ranging from 10^{-12} to 10^{-21} m^2 to be measured, corresponding to hydraulic conductivity from 10^{-5} to 10^{-14} m/s for water at 20 °C. Measurement is carried out in a steady flow state with a moderate injection pressure of 1.5 MPa.

For a complete description of this test see also Refs. [2,15,16].

This method has been checked in many occasions when it was possible to directly measure the flow [9,16]. The following equation has been used to calculate the intrinsic permeability:

$$K_x = \frac{\mu Q_m}{S} \frac{2hP_m}{\left(P_m^2 - P_o^2\right)} \tag{4}$$

where S is the sample cross section, h is the length of the sample, P_o is the draining pressure, P_m is the constant mean injection pressure, Q_m is the mean entry gas flow and μ is the gas viscosity.

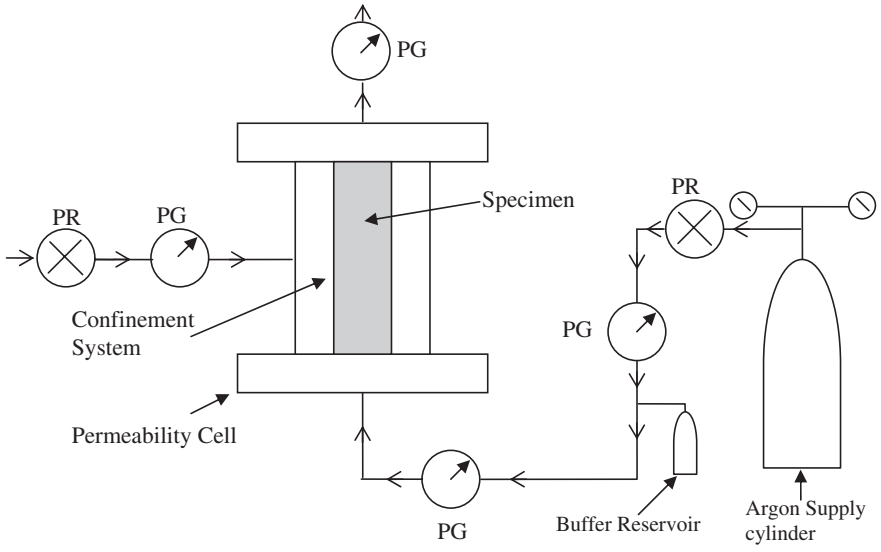

Fig. 5. Schematic diagram of the experimental setup used for gas permeability measurements.

4. Relationship between UPV, porosity and permeability

The theoretical relationship between ultrasonic propagation and material durability parameters is based on a simple model proposed by Yaman et al. [32]. First, the longitudinal and shear wave velocities are related to the elastic moduli and density by well-known formulas [1]:

$$V_L = \sqrt{\frac{E}{\rho}\frac{1-v}{(1+v)(1-2v)}} \quad V_T = \sqrt{\frac{E}{\rho}\frac{1}{2(1+v)}} \tag{5}$$

where E is the dynamic Young's modulus, v is the Poisson ratio and ρ is the density. The underlying assumption for Eq. (5) is the homogeneity of the medium as regards to the ultrasonic wave, i.e. the wavelength must be much larger than the grain size.

Next, the relationship between Young's modulus and porosity p is taken in the form of a power law [5]:

$$E = E_0(1-p)^c \tag{6}$$

where c is an empirical fitting parameter and E_0 is the Young's modulus of the material at zero porosity (in what follows, index '0' will refer to the zero-porosity material). As density is related to porosity by:

$$\rho = \rho_0(1-p) \tag{7}$$

and neglecting the influence of porosity on Poisson ratio, i.e. $v = v_0$ for a given value of water content, insertion of Eqs. (6) and (7) into Eq. (5) yields:

$$V_L = V_{L0}(1-p)^a \quad V_T = V_{T0}(1-p)^a \tag{8}$$

where $V_{L0} = \sqrt{\frac{E_0}{\rho_0}\frac{1-v_0}{(1+v_0)(1-2v_0)}}$, $V_{T0} = \sqrt{\frac{E_0}{\rho_0}\frac{1}{2(1+v_0)}}$ and $a = \frac{c-1}{2}$.

For low porosity values, Eq. (8) can by approximated by the following linear relationships:

$$V_L = V_{L0}(1-bp) \quad V_T = V_{T0}(1-bp). \tag{9}$$

According to Shkolnik et al. [28], parameter b is related to Poisson ratio at zero porosity by:

$$b = 15\frac{1-v_0}{7-5v_0}. \tag{10}$$

Finally, the porosity–permeability relationship is derived from a simple model, assuming that for fluid flow, the system of open pores is equivalent to a set of parallel circular channels of diameter d directed along the macroscopic fluid flow [30]:

$$k = \frac{pd^2}{32}. \tag{11}$$

Combining Eqs. (9) and (11), a linear relationship between permeability and UPV can be derived:

$$k = \frac{d^2}{32b}\frac{\Delta V_{L,T}}{V_{L,T0}} \tag{12}$$

where $\frac{\Delta V_{L,T}}{V_{L,T0}}$ corresponds to the variation of UPV of longitudinal or shear wave relative to the zero-porosity value. Eqs. (8), (9) and (12) represent the theoretical model relating UPV with porosity and permeability. In the following sections, they will be compared with empirical relationships obtained from measurements performed on mortar samples.

5. Results and discussions

In order to investigate the effect of porosity on ultrasonic parameters and permeability, each sample of mortar was subjected to the three kinds of tests described in Section 3. Various levels of porosity were obtained using mortar with seven values of water/cement (w/c) ratio: 0.3, 0.35, 0.4, 0.45, 0.5, 0.55 and 0.6. Through the saturation and drying process described in Section 2, water content was also taken as a parameter, with three different levels: dry, partially and fully saturated. For each w/c ratio and water saturation level, the presented result is an average of measurements performed on three samples taken from the same core.

5.1. Porosity

Fig. 6 illustrates the variation of porosity with w/c ratio. As expected, porosity is observed to increase with w/c ratio. The relationship is obviously not linear. Porosity values range from 8% for the lowest w/c ratio to 13.5% for the highest.

5.2. Ultrasonic parameters

Fig. 7 displays the variation of longitudinal and shear wave velocity versus porosity, for dry, partially and fully saturated samples. It can be noticed that velocity is affected by both porosity and water content. For a given value of water content, a significant decrease of velocity with increasing porosity is observed for both waves. As an example, the reduction of velocity, for the fully saturated material, is about 15% when porosity increases from 8% to 13.5%. This trend is coherent with the model described by Eq. (5), where longitudinal and shear velocities are assumed to be proportional to Young's modulus and inversely proportional to density. The decrease of velocity can be explained by the fact that, when porosity increases, Young's modulus decreases faster (as a power law,

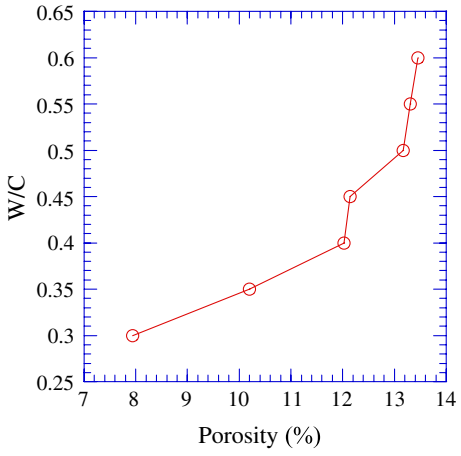

Fig. 6. Variation of porosity with water/cement ratio.

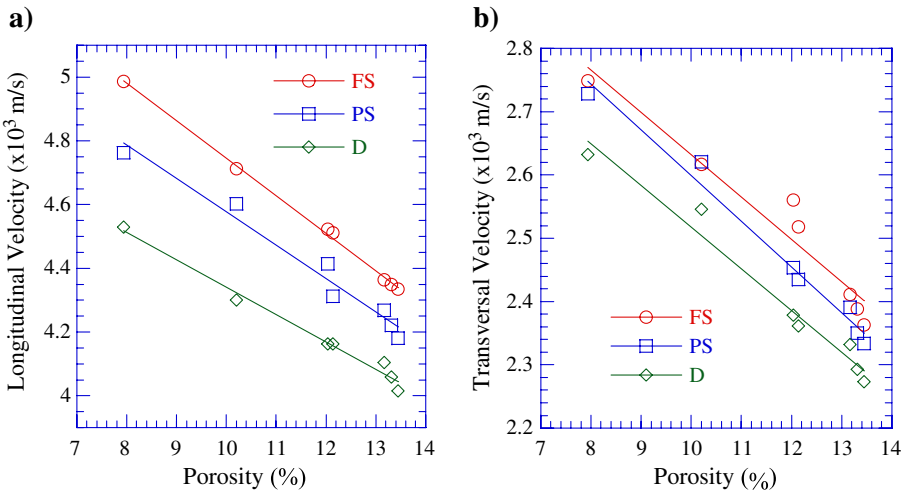

Fig. 7. Variation of ultrasonic pulse velocity versus porosity. a) Longitudinal wave; b) Shear wave.

see Eq. (6)) than density (as a linear law, see Eq. (7)). For a given value of porosity, the obtained results also show that velocity of both waves increases with water content. This was already observed by Ohdaira and Masuzawa [19]. In comparison with the dry material, the presence of water inside the pores of the saturated material provides additional stiffness. Another explanation proposed by Yaman et al. [32] and confirmed by micro-mechanical models is that velocity variation between the dry and the saturated state is due to the change of pore shape with moisture ingress into the material. As expected, longitudinal wave velocity is about two times higher than shear wave velocity. The behavior of shear wave velocity is similar to that of longitudinal wave velocity. However, the shear wave appears to be less sensitive to water content, especially when we compare the partially (PS) and fully (F) saturated samples.

Fig. 8 shows the variation of longitudinal and shear wave attenuation versus porosity, for dry, partially and fully saturated samples. For both kinds of waves, attenuation is observed to increase with porosity and water content. The ratio between shear and longitudinal attenuation is between 2 and 4, depending on porosity. The increase of attenuation slope with porosity in mortar samples was already observed by Vergara et al. [31] for the longitudinal wave, using an indirect method for measuring attenuation. Several other authors [6,33,34] reported that the presence of water in rocks decreases the quality factor, which corresponds to an increase of the attenuation slope. For porosity higher than 12%, attenuation displays a steep increase, especially for the longitudinal wave (Fig. 8a). It means that attenuation is not only sensitive to porosity, but also to a change of microstructure in the material when the w/c ratio is higher than 0.45. This steep increase of attenuation may be related to scattering of the ultrasonic wave by pores of increasing size, while the volume of pores remains almost constant compared to samples with lower w/c ratios. It is well known that, when the wavelength is much larger than the mean size $\langle D \rangle$ of scatterers, Rayleigh scattering induces attenuation proportional to $\langle D \rangle^3$ [21]. The increase of pore size with increasing w/c ratio has been reported for cement pastes [27], and similar behaviour is expected to appear in mortar. However, in order to substantiate this thesis, further studies are necessary. Mercury intrusion porosimetry (MIP) could have

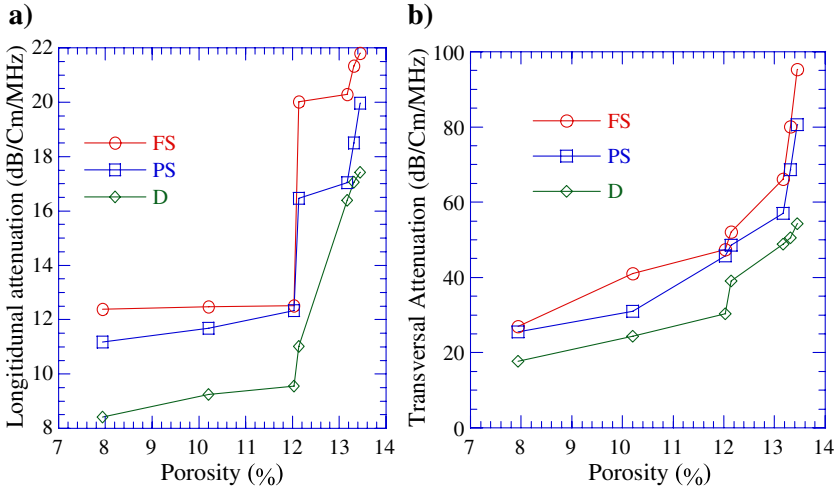

Fig. 8. Variation of ultrasonic attenuation versus porosity. a) Longitudinal wave; b) Shear wave.

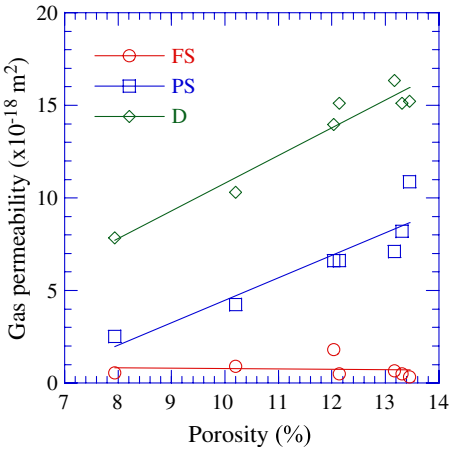

Fig. 9. Variation of permeability versus porosity.

been used to estimate pore size distribution within limitations found for cement-based materials, due to throat effects [8]. Thus, more advanced techniques, such as magnetic resonance imaging (MRI) or backscattered electron imaging, should be also considered.

5.3. Gas permeability

Results plotted on Fig. 9 present the measured gas permeability values versus porosity, for dry and partially saturated mortar samples. The dependence of permeability on porosity and water content is very significant. As an example, gas permeability increases gradually from $7 \cdot 10^{-18}$ to $16 \cdot 10^{-18}$ m^2 when the porosity increases from 8% to 13.5%. For a given value of porosity (p=13.5%), gas permeability increases from 10^{-17} to $15 \cdot 10^{-18}$ m^2, when the water content decreases from partially saturated sample to dry sample. Even if the relationship between permeability and porosity seems to be natural, we should be careful to interpret these results. Eq. (11) describes a relationship which only involves the pore diameter as a parameter. As a matter of fact, permeability doesn't depend only on porosity but also on tortuosity, specific surface, pore size distribution and connectivity of pores.

6. Correlations

6.1. UPV and porosity

The following tables present the results of linear and logarithmic regression performed on UPV values for the longitudinal (Table 2) and the shear wave (Table 3). Logarithmic regression is intended to fit the experimental data with the theoretical relationship expressed by Eq. (8), whereas linear regression corresponds to Eq. (9). Parameters V_{L0} and V_{T0}, the values of velocity at zero porosity, are estimated as the Y-intercept of the regression lines. In both tables, the correlation coefficient R is presented. All values of R are found to be higher than 0.96, which means that the simple model described by Eqs. (8) and (9) correctly describes the behavior of UPV in the range of porosity values considered (8% to 13.5%). For the longitudinal wave, model parameters V_{L0}, a and b decrease from the fully saturated to the dry state. A similar evolution is not observed for the shear wave though, since a and b remain almost constant, around 2 and 2.3 respectively, for all saturation levels. This result highlights the lower sensitivity of the shear wave to the water content mentioned earlier.

Table 2
Experimental parameters obtained from linear and logarithmic regression on the data of longitudinal wave velocity versus porosity

Water saturation level	Linear regression			Logarithmic regression		
	V_{L0}	b	R	V_{L0}	a	R
Full Saturation (FS)	5921	1.985	0.99	6013	2.25	0.99
Partial Saturation (PS)	5624	1.861	0.98	5691	2.07	0.98
Dry (D)	5201	1.653	0.99	5244	1.79	0.99

Table 3
Experimental parameters obtained from linear and logarithmic regression on the data of shear wave velocity versus porosity

Water saturation level	Linear regression			Logarithmic regression		
	V_{T0}	b	R	V_{T0}	a	R
Full Saturation (FS)	3301	2.02	0.96	3351	2.3	0.96
Partial Saturation (PS)	3321	2.173	0.99	3389	2.52	0.98
Dry (D)	3175	2.07	0.98	3230	2.37	0.98

Parameter b corresponds to the slope of the linear relationship between UPV and porosity (Eq. (9)). Table 4 compares the values estimated from linear regression of experimental data (column 3 of Tables 2 and 3) with the values derived from Eq. (10). From Eq. (5), the Poisson ratio at zero-porosity v_0 is obtained as:

$$v_0 = \frac{1}{2}\frac{1-2(V_{T0}/V_{L0})^2}{1-(V_{T0}/V_{L0})^2}. \quad (13)$$

It appears that b_{Shko} is close to the values of b_{shear} but doesn't vary as much as b_{long} with water content. However, Eq. (10) gives a reasonable value of model parameter b.

6.2. UPV and permeability

In order to compare the measured variation of UPV versus permeability with the relationship derived from the model (Eq. (12)), the variation of longitudinal and shear velocity relative to the velocity at zero porosity is presented in Fig. 10. The curve corresponding to the fully saturated material is not shown here, as the observed variation of permeability is insignificant. To evaluate the agreement of experimental data with Eq. (12), a linear regression is performed on the curves

Table 4
Comparision between values of model parameter b derived from Eq. (10) (b_{Shko}) and from linear regression of longitudinal (b_{long}) and shear (b_{shear}) velocities vs. porosity

Water saturation level	v_0	b_{Shko}	b_{long}	b_{shear}
Full Saturation (FS)	0.277	1.93	1.985	2.02
Partial Saturation (PS)	0.225	1.98	1.861	2.173
Dry (D)	0.194	2.00	1.653	2.07

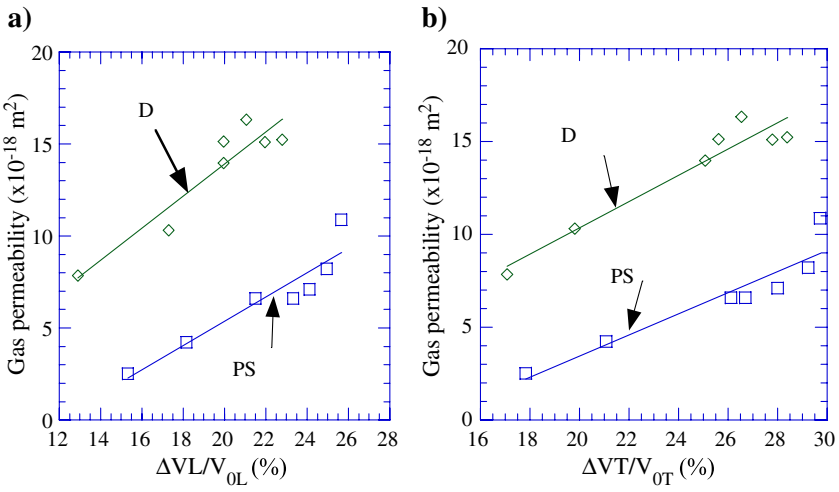

Fig. 10. Gas permeability versus relative UPV variation $\frac{\Delta V_{(T,L)}}{V_{(T,L)_0}}$. a) Longitudinal wave; b) Shear wave.

presented on Fig. 10. Results are presented in Table 5. All values of the regression coefficient R are found to be higher than 0.93, which means that the measured variation of UPV versus permeability is correctly described by a linear relationship in the range of porosity and permeability values considered. From the slope of the regression line and the values of parameter b in Table 4, it is possible to estimate the value of the mean pore diameter d. This value is found to be 70 nm for the dry material and 66 nm for the partially saturated material. When compared with data provided by Mehta and Manmohan [18], these values correspond to a correct order magnitude for micropores.

7. Conclusions

The first objective of this study was to investigate the variation of ultrasonic parameters of mortar with its porosity, permeability and water content. Ultrasonic parameters, namely pulse velocity (UPV) and attenuation (UA), were measured for longitudinal and shear waves, using wideband spectroscopy in a frequency range from 0.5 to 1 MHz. Permeability was measured by injection of a continuous gas flow through the material, under constant pressure gradient. Porosity was obtained by the gravity method, using vacuum saturation. Finally, water content was set to three different levels (dry, partial and full saturation) by adjusting the drying time of the fully saturated material. The observed variation of ultrasonic parameters is as follows:

– Pulse velocity decreases with porosity and permeability, and it increases with water content. Shear wave velocity is about half of the longitudinal wave velocity and seems to be less sensitive to the water content.
– Attenuation increases with porosity, permeability and water content. Shear wave attenuation is 2 to 4 times higher than longitudinal wave attenuation, depending on porosity.

Such trends correspond to the expected behaviour and are coherent with works published by other researchers [19,31,34]. In addition, the steep increase of attenuation beyond 12% porosity may indicate a change of microstructure, and more specifically an increase of the amount of larger pores at the expense of the volume of smaller ones.

The second objective was to establish correlations between UPV, porosity and permeability, for different values of water content, and to compare those correlations with the model proposed by Yaman et al. [32]. This model predicts a linear relationship between UPV, porosity and permeability. In the range of porosity values considered in this study, our experimental data fit well with the linear model. In addition, the model parameters that can be derived from experimental data correspond approximately with the expected values. The slope of the UPV versus porosity relationship is found to be close to 2, as predicted by Popovics et al. [26]. The diameter of pores, which can be estimated from the slope of the UPV versus permeability relationship, yields a reasonable order of magnitude. However, it should be noted that low porosity values in a narrow range (from 8% to 13.5%) are considered. The linear approximation (Eq. (10)) of the power law (Eq. (8)) may not be valid for higher porosity values.

Given the obtained promising correlations for mortars, further studies are necessary to establish whether the non-

Table 5
Results of linear regression of data from Fig. 10: Slope of the regression line (Slope), regression coefficient (R) and pore diameter (d)

Water content	Longitudinal wave			Shear wave		
	Slope (10^{-18} m^2)	R	d (nm)	Slope (10^{-18} m^2)	R	d (nm)
Partial saturation (PS)	65.952	0.94	66	56.854	0.93	67
Dry (D)	87.181	0.94	70	70.729	0.96	73

destructive ultrasonic measurements may be useful to infer durability indices (namely, porosity and permeability) of concrete structures studied in situ.

Acknowledgements

This study was funded in part by the French Ministry of Infrastructure and the French Ministry of Education and Research through the "Réseau Génie Civil et Urbain" (RGCU). Thanks to Ecole Centrale de Lille for supporting the stays of Pr. Kaczmarek as an invited professor.

References

[1] J.D. Achenbach, Wave Propagation in Elastic Solids, American Elsevier, Amsterdam, 1973.
[2] AFREM Durabilité des bétons. Essai de perméabilité aux gaz du béton durci: mode opératoire recommandé, 1996.
[3] D. Breysse, B. Gerard, Modelling of permeability in cement-based materials: Part 1. Uncracked medium, Cement and Concrete Research 27 (5) (1997) 761–775.
[4] J.H. Bungey, S.G. Millard, Testing of Concrete in Structures, 3rd edition, Chapman & Hall, 1996.
[5] N.I. Christensen, Seismic velocities, in: Robert S. Carmichael (Ed.), Handbook of Physical Properties of Rocks, vol. II, CRC press, 1982.
[6] V.A. Clark, B.R. Tittmann, T.W. Spencer, Effect of volatiles on attenuation (Q-1) and velocity in sedimentary rocks, Journal of Geophysical Research 85 (1980) 5190–5198.
[7] O. Coussy, Mécanique des milieux poreux, Editions Technip, Paris, 1990.
[8] S. Diamond, Mercury porosimetry. An appropriate method for the measurement of pore size distributions in cement-based materials, Cement and Concrete Research 30 (2000) 1517–1525.
[9] A. Dinku, H.W. Reinhardt, Gas permeability coefficient of cover concrete as a performance control, Materials and Structures 30 (1997) 387–393.
[10] F. Eggers, U. Kaatze, Broad-band ultrasonic measurement techniques for liquids, Measurement Science & Technology 7 (1996) 1–19.
[11] M. Goueygou, S. Ould Naffa, B. Piwakowski, A. Fnine, F. Buyle-Bodin, Measurement of ultrasonic attenuation and Rayleigh wave dispersion for testing concrete with subsurface damage, Proc. of IEEE UFFC Symposium, Münich, Germany, 2002.
[12] M. Goueygou, B. Piwakowski, S. Ould Naffa, F. Buyle-Bodin, Assessment of broadband ultrasonic attenuation measurements in inhomogeneous media, Ultrasonics 40 (2002) 77–82.
[13] M.G. Hernandez, M.A.G. Izquierdo, A. Ibanez, J.J. Anaya, L.G. Gomez-Ullate, Porosity estimation of concrete by ultrasonic NDT, Ultrasonics 38 (2000) 531–536.
[14] R. Iffly, Etude de l'écoulement des gaz dans les milieux poreux, Revue IFP XI (6) (1956) 757–1018.
[15] Loosveldt H. Etude Expérimentale des comportements hydrauliques et poromecaniques d'un mortier sain ou dégradé chimiquement. Thesis, Ecole Centrale de Lille, 2002.
[16] H. Loosveldt, Z. Lafhaj, F. Skoczylas, Experimental study of gas and liquid permeability of a mortar, Cement and Concrete Research 32 (2002) 1357–1363.
[17] V.M. Malhotra, N.J. Carino, Handbook on Nondestructive Testing of Concrete, CRC Press, Boca Raton, 1991.
[18] P.K. Mehta, D. Manmohan, Pore size distribution and permeability of hardened cement paste, in: 7^{e} Congrès International de la Chimie des Ciments, Paris, vol. 3, 1980, pp. 1–11.
[19] E. Ohdaira, N. Masuzawa, Water content and its effect on ultrasound propagation in concrete — the possibility of NDE, Ultrasonics 38 (2000) 546–552.
[20] S. Ould Naffa, M. Goueygou, B. Piwakowski, F. Buyle-Bodin, Detection of chemical damage in concrete using ultrasound, Ultrasonics 40 (2002) 247–251.
[21] E.P. Papadakis, Revised grain-scattering formulas and tables, Journal of the Acoustical Society of America 37 (4) (1965) 703–710.
[22] E.P. Papadakis, Buffer-rod for ultrasonic attenuation measurements, Journal of the Acoustical Society of America 44 (5) (1968) 1437–1441.
[23] E.P. Papadakis, K.A. Fowler, L.C. Lynnworth, Ultrasonic attenuation by spectrum analysis of pulses in buffer rods: method and diffraction correction, Journal of the Acoustical Society of America 53 (5) (1973) 1336–1343.
[24] S. Popovics, L. Joseph, S. John, The behavior of ultrasonic pulses in concrete, Cement and Concrete Research 20 (2) (1990) 259–270.
[25] S. Popovics, Strength and Related Properties of Concrete: a Quantitative Approach, John Wiley & Sons, New York, 1998.
[26] J.S. Popovics, W. Song, J.D. Achenbach, J.H. Lee, R.F. Andre, One-sided stress wave velocity measurement in concrete, Journal of Engineering Mechanics 24 (12) (1998) 1346–1353.
[27] D.M. Roy, P.W. Brown, D. Shi, B.E. Scheetz, W. May, Concrete microstructure porosity and permeability, Strategic Highway Research Program, Report SHRP-C-628, National Research Council, Washington, DC, 1993.
[28] I.E. Shkolnik, O.C. Udegbunam, H.M. Aktan, Ultrasonic methods of evaluating concrete permeability, Proc. of the Conference on NDT in Civil Engineering, British Institute of NDT, University of Liverpool, 1997, pp. 111–120.
[29] K. Tharmaratnam, B.S. Tan, Attenuation of ultrasonic pulse in cement concrete, Cement and Concrete Research 20 (3) (1990) 335–345.
[30] O. Udegbunam, I. Yaman, H. Aktan, T. Hohm, Developing a rapid measure of concrete permeability for use in QA/QC specifications, Transportation Research Board, 78th Annual Meeting, January 10–14, Washington D.C., 1999.
[31] L. Vergara, R. Miralles, J. Gosalbez, F.J. Juanes, L.G. Ullate, J.J. Anaya, M.G. Hernandez, M.A.G. Izquierdo, NDE ultrasonic methods to characterise the porosity of mortar, NDT & E International 34 (2001) 557–562.
[32] I.O. Yaman, H.M. Aktan, N. Hearn, Active and non-active porosity in concrete: Part II. Evaluation of existing models, RILEM Journal of Materials and Structures 35 (246) (2002) 110–116.
[33] K. Winkler, A. Nur, Pore fluids and seismic attenuation in rocks, Geophysical Research Letters 61 (1979) 1–4.
[34] K. Winkler, A. Nur, Seismic attenuation: effects of pore fluids and frictional sliding, Geophysics 47 (1) (1982) 1–15.